energies

MDPI

Article

Deep Learning Algorithm for Solving Interval of Weight Coefficient of Wind–Thermal–Storage System

Yanchen Liu and Minfang Peng *

College of Electrical and Information Engineering, Hunan University, Changsha 410082, China; liuyanchen@hnu.edu.cn

* Correspondence: pengminfang@hnu.edu.cn

Abstract: Under the premise of ensuring the safe and stable operation of a wind–thermal–storage power system, this paper proposes an optimization model aimed at improving its overall economic efficiency and effectively reducing the peak-to-valley load difference. The model transforms the multi-objective optimization problem to solve a feasible interval of weight coefficients. We introduce a novel fusion model, where a Convolutional Neural Network (CNN) is melded with a Long Short-Term Memory Network (LSTM) to form the target network structure. Additionally, for datasets with limited samples, we incorporate a Self-Attention Mechanism (SAM) into the Model-Agnostic Meta-Learning (MAML). Ultimately, we build an MAML-SAM-CNN-LSTM network model to solve the interval of weight coefficients. An arithmetic validation of a modified IEEE 30-node system demonstrates that the MAML-SAM-CNN-LSTM network proposed in this paper can adeptly solve the feasible intervals of weight coefficients in the optimization model of the wind-thermal storage system. This is achieved under the constraints of the specified wind-thermal storage power system operation indexes. The evaluation indexes of the network model, including its accuracy, precision, recall, and F1 score, all exceed 98.72%, 98.57%, 98.30%, and 98.57%, respectively. This denotes a superior performance compared to the other three network models, offering an effective reference for optimizing decision-making and facilitating the enhanced realization of multi-objective, on-demand scheduling in the wind-thermal storage power system.

Keywords: MAML-SAM-CNN-LSTM network; deep learning; wind–thermal–storage system

check for updates

Citation: Liu, Y.; Peng, M. Deep Learning Algorithm for Solving Interval of Weight Coefficient of Wind–Thermal–Storage System. *Energies* **2024**, *17*, 1082. https://doi.org/10.3390/en17051082

Academic Editor: Marco Marengo

Received: 12 January 2024
Revised: 7 February 2024
Accepted: 21 February 2024
Published: 24 February 2024

Copyright: © 2024 by the authors. Licensee MDPI, Basel, Switzerland. This article is an open access article distributed under the terms and conditions of the Creative Commons Attribution (CC BY) license (https://creativecommons.org/licenses/by/4.0/).

1. Introduction

Due to the continuous increases in electricity consumption and environmental concerns, governments around the world have issued many incentive policies for renewable energy, significantly promoting their development and utilization [1]. However, when renewable energy is integrated into the power system at a large scale, its instability poses a challenge to the safety and reliability of the power grid. Energy storage provides energy with the ability to time-shift, enabling the storage of excess generation during periods of low demand (load valleys) and the injection of power into the grid during periods of high demand (load peaks). Therefore, leveraging energy storage is an attractive solution, which can mitigate the uncertainty associated with renewable energy generation. The ensuing challenge lies in coordinating the output of renewable energy (wind power in this paper), energy storage, and thermal power units to optimize the operation of the wind-thermal storage system.

A power system scheduling that is solely based on economic objectives falls short in addressing the requirements stemming from the evolution of the power industry and low-carbon environmental protection [2]. Therefore, the multi-objective optimization of multi-energy systems has become a hot research topic. Ref. [3] investigates the game relationship between integrated operating costs and the wind abandonment of a hybrid generation system, including thermal power units, wind farms and battery storage. Ref. [4]

developed a multi-objective scheduling model for an integrated energy system, considering two perspectives: cost and pollutant emissions. Ref. [5] considers the minimization of net cost and the probability of power supply loss for the multi-objective co-optimization of a wind–PV–storage hybrid power system. The choice of objective function in the optimization model directly mirrors the diverse requirements of decision-makers regarding the system's operational performance. Given the potential for wind power with anti-peaking characteristics to become connected to the grid and increase the peak-to-valley difference, this paper is expected to reduce the level of net load fluctuations in the system.

It can be seen that the objective function in the optimization model primarily includes two types, economic objectives and non-economic objectives, which frequently conflict with each other [6]. Therefore, determining the weights of each attribute in the multi-attribute decision space is crucial, and exploring optimization algorithms for this purpose is also highly significant.

At present, to balance multiple objectives, the most widely used methods include the weighted sum method [7,8], game theory [9,10], and various meta heuristic algorithms [11,12]. Ref. [13] proposed an optimal eco-emission scheduling model for the distribution network, considering demand response, and solved the problem using the weighted sum method and fuzzy decision making. Ref. [14] addressed multi-objective optimization problems by using the weighted sum method combined with the constraint method to minimize the cost and carbon dioxide emissions of regional heating systems. Ref. [15] applied the weighted sum method to establish a multi-objective function for hybrid energy systems, and used the entropy weight method as a quantitative method to calculate the weight factors, improving the objectivity of decision-making. The weighted sum method can transform a high-dimensional, multi-objective, optimization problem into a low-dimensional problem, greatly simplifying the solving process [16], but the correlation between changes in weight coefficients and conflicting objectives has not been analyzed. Ref. [17] proposed using game theory to solve the optimization operation of microgrids, and obtained a multi-objective equilibrium result that effectively reduces pollution without increasing the costs. Ref. [18] proposed an optimization algorithm based on potential game theory, which could achieve coordination in terms of the economy, environment, and satisfaction of the microgrid. However, because it requires the calculation of game theory objects individually, the game-theory-based approach is more suitable for small-scale microgrids. Applying it to larger grid sizes would significantly extend the computational time. Ref. [19] employed a non-dominated sorting genetic algorithm to optimize three objectives simultaneously: operating costs, carbon emissions, and customer dissatisfaction, obtaining Pareto fronts. Subsequently, the TOPSIS method was utilized to determine the optimal solution. Ref. [20] used a multi-objective differential evolution algorithm to solve the dynamic economic scheduling model for wind–photovoltaic–storage systems. Targeting the maximum economic benefits and minimal interaction fluctuations in the power grid, Ref. [21] used a predictive variation particle swarm optimization to derive the Pareto solution set. Based on this, the final solution was selected using the membership function. Although metaheuristic methods have an excellent performance when identifying global optimal solutions, their solving speed is slow due to the complex coding and large number of iterative calculations. In addition, for problems with complex Pareto fronts, the uniform distribution of solutions can not be guaranteed [22,23].

Each of the above methods for multi-objective optimization has its own characteristics. However, they do not consider the preferences of decision-makers or operators, so the optimal solutions are only fixed values that satisfy the objective model. Whether the plan in actual scheduling should be adopted or adjusted still largely depends on subjective judgment. Therefore, this article proposes a deep learning algorithm to deduce the reasonable range of system operating parameters (weight coefficients) based on the preferences of decision-makers or operators, i.e., the prescribed system indicator threshold. This facilitates dispatchers in determining whether to adjust the power generation strategy to achieve system optimization under the preferred objectives, and has greater value and significance in

engineering applications. The innovations and contributions of this article are summarized as follows:

(1) The establishment of a multi-objective optimization model that considers both the peak load shifting and economic costs.
(2) An exploration of the correlation between changes in weight coefficients and conflicting objectives.
(3) The development of an MAML-SAM-CNN-LSTM network, rooted in deep learning algorithms, to deduce the reasonable range of system operating parameters (weight coefficients) in terms of the prescribed indicator threshold, which can suit the decision-makers' or operators' preferences and achieve on-demand coordination between system economy and peak load shifting.

2. Multi-Objective Optimization Model

For different hybrid systems, the objective function, decision variables, and constraints of the mathematical model are different, but the general minimization problem of M objectives can be expressed mathematically, as follows:

$$\min F(x) = \min[f_1(x), f_2(x), \cdots, f_M(x)]^T \quad (1)$$

$$g_k(x) = 0;\ k = 1, 2, \cdots, K \quad (2)$$

$$h_j(x) \geq 0;\ j = 1, 2, \cdots, J \quad (3)$$

where $x = [x_1, x_2, \ldots, x_s]^T$, and s is the dimension of the variable in the decision space. $f_i(x)$ is the i-th objective function, $g_k(x)$ is the k-th equality constraint, and $h_j(x)$ is the j-th inequality constraint.

The data show that, in multi-objective optimization articles, researchers focus on two indicators: economy and reliability [24]. Therefore, Equation (1) can be rewritten to an expression including the weight coefficient, as follows:

$$\min F(x) = \min[f_e(x) + \omega f_r(x)] \quad (4)$$

where $f_e(x)$ is the economic target; $f_r(x)$ is the non-economic target (peak load shifting target in this paper); ω is the weight coefficient used to balance the goals of peak load shifting and system economy. Based on Equation (4), this article harmonizes the mutual game of two targets. We employed deep learning algorithms to determine the feasible interval of the ω and explore the impacts of ω variations on the operation of the wind–thermal–storage system.

3. Wind–Thermal–Storage System Model

The wind–thermal–storage system studied in this article mainly consists of conventional thermal power generators, renewable energy (wind turbines), grid-side battery stations, and power loads.

3.1. Objective Function

The objective function is guided by different evaluation indicators and will have different impacts on the system's optimization results. The optimization objectives of the model proposed in this article include two parts: system economic cost and peak load shifting. During the dispatch cycle, wind power can be accommodated to the maximum extent possible based on the actual load of the system, and efforts are made to smooth the net load curve, provided that operational constraints are met. At the same time, by reasonably allocating the outputs of units within the system, the operating cost of the entire wind–thermal–storage system is minimized.

In the constructed optimal model, the peak load shifting goal is converted into the load-balancing economic cost and added to the total costs. Consequently, the system

operating costs and net load fluctuations can be optimized simultaneously to minimize the total system costs. Equation (4) is rewritten as follows:

$$\min F = f_G + f_{cw} + f_E + \omega f_{pls} \tag{5}$$

where f_G is the operating cost of the conventional thermal power unit, f_{cw} is the wind abandonment cost, f_E is the battery charging and discharging cost, and f_{pls} is the economic cost function for peak load shifting. Different system economies and peak load shifting effects can be achieved by dynamically adjusting ω.

(1) The operation cost of the conventional thermal power units can be expressed as the costs of coal consumption:

$$f_G = \sum_{t=1}^{N_T} \sum_{i=1}^{N_G} a_i P_{G,i,t}^2 + b_i P_{G,i,t} + c_i \tag{6}$$

where a_i, b_i, and c_i are the coefficients of the coal consumption curve of unit i. $P_{G,i,t}$ is the active output of conventional unit i in time period t. N_T is the number of time steps in a scheduling period and, in this paper, the scheduling period is set as one day, and the time step is 1 h, i.e., $N_T = 24$. N_G is the number of conventional units.

(2) To increase the acceptance of wind power and reduce its abandonment rate, an abandonment penalty cost is established:

$$f_{cw} = \sum_{t=1}^{N_T} \sum_{j=1}^{N_W} C_{cw,j} \left(P_{fw,j,t} - P_{w,j,t} \right) \tag{7}$$

where $C_{cw,j}$ is the wind abandonment cost coefficient in wind farm j. $P_{fw,j,t}$ and $P_{w,j,t}$ are the predicted and dispatched wind power of wind farm j at time t, respectively. N_W is the number of wind farms.

(3) Assuming that the operator owns the energy storage system, the cost of energy storage in this study is only the operation cost:

$$f_E = \sum_{t=1}^{N_T} \sum_{k=1}^{N_E} C_{E,k} (P_{EC,k,t} + P_{ED,k,t}) \tag{8}$$

where $C_{E,k}$ is the operation cost coefficient of storage battery k. $P_{EC,k,t}$ is the charging power of storage battery k at time t, and $P_{ED,k,t}$ is the discharging power (both of them are positive). N_E is the amount of energy storage.

(4) In this article, the sum of squared net load changes in consecutive time intervals characterizes net load fluctuations, representing the goal of peak shaving. Then, the charging–discharging power of energy storages and the wind power outputs is regarded as the generalized electric load. The sum of the electrical loads and battery charging power belongs to the load side, and the sum of the battery discharging power and wind power output belongs to the generation side; then, the difference between them is defined as the net load.

$$P_{net,t} = \left(\sum_{i=1}^{N_L} P_{L,i,t} + \sum_{k=1}^{N_E} P_{EC,k,t} \right) - \left(\sum_{k=1}^{N_E} P_{ED,k,t} + \sum_{j=1}^{N_W} P_{w,j,t} \right) \tag{9}$$

where $P_{net,t}$ is the system net load at moment t, $P_{L,i,t}$ is the active power of load node i at time t, and N_L is the number of load nodes.

Due to the disparity in meaning and magnitude between the peak shaving objective and the operating cost objective function, an economic function is incorporated to map the peak shaving objective to the economic dimension.

$$f_{pls} = \sum_{t=1}^{N_T} f_b (P_{net,t} - P_{net,t-1}) \tag{10}$$

where $f_b(x) = 0.5x^2$ is commonly used in the load leveling problem [25].

The constraints encompass various aspects, including limitations on system operation, and the operation of conventional units, wind turbines, and energy storage systems.

$$\sum_{i=1}^{N_G} P_{G,i,t} + \sum_{j=1}^{N_W} P_{w,j,t} = \sum_{i=1}^{N_L} P_{L,i,t} + \sum_{k=1}^{N_E} P_{EC,k,t} - \sum_{k=1}^{N_E} P_{ED,k,t} \tag{11}$$

$$P_{G,i}^{min} \le P_{G,i,t} \le P_{G,i}^{max} \tag{12}$$

$$P_{G,i}^{down} \cdot \Delta t \le P_{G,i,t} - P_{G,i,t-1} \le P_{G,i}^{up} \cdot \Delta t \tag{13}$$

$$0 \le P_{w,j,t} \le P_{fw,j,t} \tag{14}$$

$$SOC_{k,t} = SOC_{k,t-1} + \left(\frac{\eta_{EC,k} P_{EC,k,t} \Delta t}{S_{EN,k}} - \frac{P_{ED,k,t} \Delta t}{\eta_{ED,k} S_{EN,k}} \right) \times 100\% \tag{15}$$

$$SOC_k^{min} \le SOC_{k,t} \le SOC_k^{max} \tag{16}$$

$$P_{EC,k}^{min} \le P_{EC,k,t} \le P_{EC,k}^{max} \tag{17}$$

$$P_{ED,k}^{min} \le P_{ED,k,t} \le P_{ED,k}^{max} \tag{18}$$

where Equation (11) represents the balance constraint of active power in the hybrid system. Equation (12) represents the limits of the generator active power; $P_{G,i}^{min}$ and $P_{G,i}^{max}$ are the minimum and maximum active power of thermal unit i, respectively. Equation (13) is the ramping constraints; $P_{G,i}^{down}$ and $P_{G,i}^{up}$ represent the maximum downhill rate and maximum uphill rate of thermal power unit i. Δt is the time interval, and Δt = 60 min in this paper. Equation (14) is the constraint of the grid-connected wind power. Equations (15)–(18) denote the operation constraints of the energy storage batteries. $SOC_{k,t}$ is the State of Charge (SOC) parameter of battery k at time t, $\eta_{EC,k}$ and $\eta_{ED,k}$ denote the charging and discharging efficiencies of battery k, and $S_{EN,k}$ is the rated capacity of battery k. SOC_k^{max} and SOC_k^{min} are the maximum and minimum SOC values of battery k, respectively. $P_{EC,k}^{min}$ and $P_{EC,k}^{max}$ are the lower and upper limits of the charging power of battery k, respectively. $P_{ED,k}^{min}$ and $P_{ED,k}^{max}$ are the lower and upper limits of the discharging power of battery k, respectively.

3.2. System Operation Evaluation Indicators

To evaluate and adjust the operating status of the wind–thermal–storage system, this article provides two types of evaluation indicators.

The economic indicator, denoted as the system's total cost, F, can be calculated using Equation (5).

The peak load shifting evaluation index primarily describes the degree of flattening of the net load curve on a given time scale, and it can be characterized by the net load valley–peak coefficient δ. The definition of δ is the ratio of the minimum net load to the maximum in a wind–thermal–storage system during a dispatch cycle. This ratio is calculated using the following formula:

$$\delta = \frac{P_{net}^{min}}{P_{net}^{max}} \tag{19}$$

where P_{net}^{min} is the minimum value of the net load in a dispatch cycle, and P_{net}^{max} is the maximum.

Under system constraints, for any given ω, the minimum total cost can be obtained by solving Equation (5) through an optimization algorithm. At the same time, the operating parameters of thermal power, wind power, and energy storage can be calculated, and further the net load valley–peak coefficient δ, so the values of (F, δ) can be obtained. For different ω values, the corresponding values of (F, δ) can obtained. However, when traversing ω to acquire the set of (F, δ), the computing power and time costs that are involved are quite significant and unrealistic.

Grid dispatching staff often aspire to control (F, δ) within a certain range; that is, under the premise of the safe and stable operation of the power grid, they aim to effectively improve the overall economy and reduce the peak–valley load difference. Therefore, this article expects that ω can be solved under any given system operating indicator threshold (F, δ). If there is no solution for ω, this implies that the expectation of achieving (F, δ) simultaneously is unreasonable. However, if there are multiple ω solutions, all satisfying the (F, δ) requirement, the multi-objective optimization problem can be transformed into a feasible interval problem to solve ω.

4. MAML-SAM-CNN-LSTM Neural Network

Given the limited data in the (F, δ) set, we introduced Model-Agnostic Meta- Learning (MAML) into the target network structure of the Convolutional Neural Network-Long Short-Term Memory Network (CNN-LSTM) to address the challenges posed by a small sample size. Additionally, the Self-Attention Mechanism (SAM) was incorporated to enhance the generalization performance of the neural network and its adaptability to new tasks, resulting in the construction of the MAML-SAM-CNN-LSTM network.

4.1. CNN-LSTM Network

CNN can extract the features hidden in input data, reduce data dimensions, and prevent overfitting. It is commonly used for regression or classification tasks [26].

The feature extraction equation for one-dimensional convolution is as follows:

$$Y = L_R(W_l * X + B_l) \tag{20}$$

where Y is the feature extracted by 1D convolution, L_R is the activation function LeakRelu, W_l is the weight matrix, and B_l is the bias matrix. X is the sets of input sequences, namely the sets of net load valley–peak coefficients and the total costs. * is convolution operation.

The Recurrent Neural Network (RNN) is prone to gradient vanishing and exploding during the training process and, over time, information that is input from the past will gradually be forgotten [27]. The LSTM network [28] adds three gate structures (forget gate fg, input gate ig, and output gate og) and cell state (ct) on the basis of RNN. The new information that should be retained in ct at the current moment is determined by ig; information that needs to be forgotten in ct is determined by fg; information that needs to be output from ct and input at the next moment is determined by og. The expressions for the three gates, respectively, are as follows:

$$fg_t = \sigma\{W_{fg}[h_{t-1}, x_t] + b_{fg}\} \tag{21}$$

$$ig_t = \sigma\{W_{ig}[h_{t-1}, x_t] + b_{ig}\} \tag{22}$$

$$og_t = \sigma\{W_{og}[h_{t-1}, x_t] + b_{og}\} \tag{23}$$

where fg_t denotes the output vector of the forget gate, ig_t denotes the output vector of the input gate, and og_t denotes the output vector of the output gate. σ denotes the sigmoid activation function. h_{t-1} denotes the output of LSTM unit at a previous time, and x_t denotes the input of LSTM unit at the current time. W_{fg}, W_{ig}, W_{og}, and b_{fg}, b_{ig}, and b_{og} denote the weights and biases, respectively, to be learned during training.

The inputs for of LSTM at the next moment are ct_t and h_t, and the expression is as follows:

$$\widetilde{C}_t = \tanh\{W_c[h_{t-1}, x_t] + b_c\} \tag{24}$$

$$ct_t = fg_t \odot ct_{t-1} + ig_t \odot \widetilde{C}_t \tag{25}$$

$$h_t = og_t \odot \tanh(ct_t) \tag{26}$$

where $\widetilde{C}_t$ represents the candidate information, tanh represents the hyperbolic tangent activation function, and W_c and b_c the represent weights and biases of the information; $\odot$ denotes the element-wise product (Hadamard product).

In the paper, the spatial features of (F, δ) are extracted by CNN, and the time characteristics of the input data (F, δ) are extracted using LSTM. The structure of the used CNN-LSTM network is shown in Figure 1.

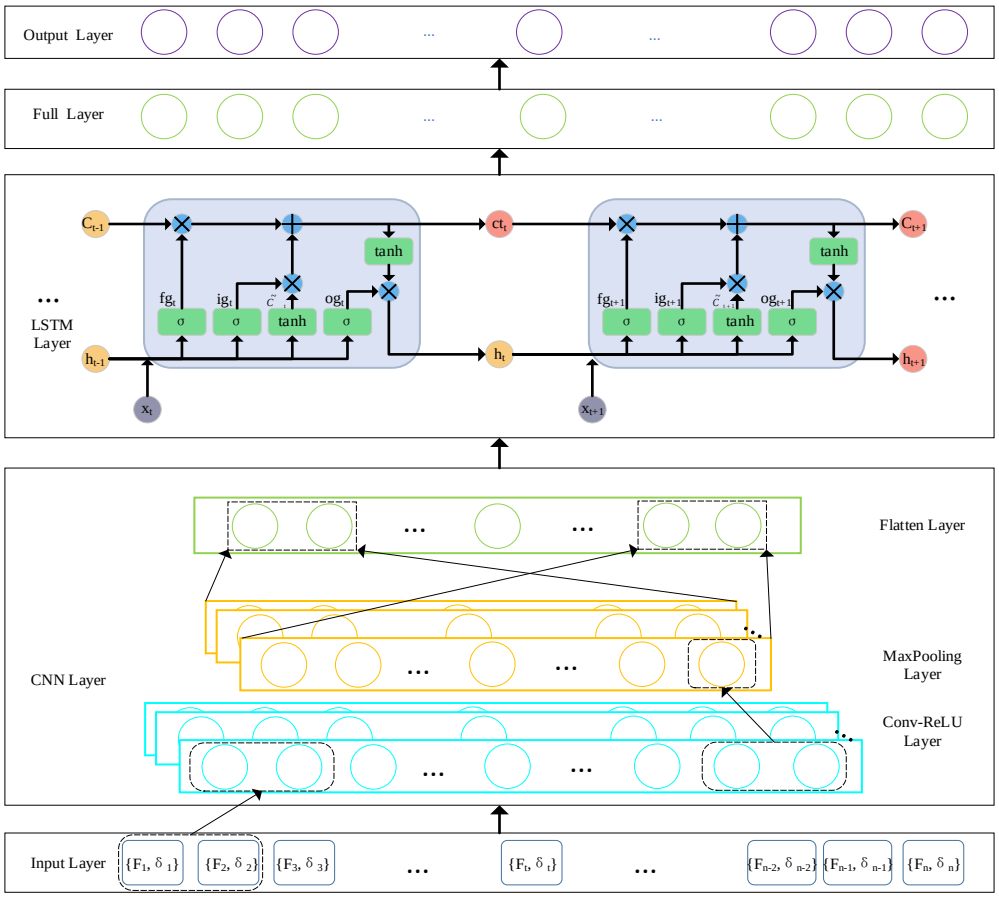


Figure 1. Network structure of CNN-LSTM.

4.2. MAML-SAM Network

4.2.1. MAML Network

According to the optimization model of the wind–thermal–storage system established in this article, for each weight coefficient ω, there is a corresponding total cost and valley–peak coefficients (F, δ). However, in reality, it is not possible to sequentially substitute each ω into the model and calculate the corresponding set of operational evaluation indicators. Therefore, due to the limited computing power and time costs, the obtained dataset samples are relatively small.

Most deep learning networks require large-scale datasets for training, and when faced with small amounts of data, they often have a poor model performance [29]. In order to address the small sample problem, and improve the generalization performance of the neural network and its adaptability to new tasks, this paper introduces MAML [30], which is executed in two stages: meta training and meta testing [31,32]. The goal of the meta training stage is to find an effective meta initialization, which will be used as the starting point for adaptive optimization parameters in the meta testing stage so that the model can effectively solve new tasks with only a small number of annotated samples.

First, the training task set $D^{\text{meta-train}}$ and the testing task set $D^{\text{meta-test}}$ are constructed based on the dataset. In the meta training stage, several training tasks T^{train} are extracted from $D^{\text{meta-train}}$, and the data in each training task T_i^{train} are partitioned into a support set T_{si}^{train} and a query set T_{qi}^{train}. As network f_θ is subjected to initialization parameter θ, the initialization parameter needs to be updated from θ to θ_i', which is obtained through one or more gradient descent. In the MAML algorithm, gradient calculations are performed on each Tsitrain using the following formula:

$$\theta_i' = \theta - \alpha \nabla L_{T_{si}^{\text{train}}}(f_\theta) \tag{27}$$

where α is the learning rate, $L_{T_{si}^{\text{train}}}$ denotes the loss on the support set T_{si}^{train} of the training task, and $\bigtriangledown$ represents the gradient operation. After gradient updating, the parameter is obtained.

Then, the effects of θ_i' on the model are tested for the query set T_{qi}^{train} of all training tasks. The goal of the meta training stage is to minimize the sum of model losses across all T_{qi}^{train}:

$$\min \sum_{T_{qi}^{\text{train}}} L_{T_{qi}^{\text{train}}}(f_{\theta_i'}) \tag{28}$$

Next, the second updating of model parameter θ is performed using the following formula:

$$\theta \leftarrow \theta - \beta \nabla L_{T_{qi}^{\text{train}}}(f_{\theta_i'}) \tag{29}$$

where β is a hyperparameter.

In the meta training stage, after two gradient updates, the parameter θ, which performed well on all tasks, is identified and used in the meta testing phase to enable the model to make accurate predictions even with small amounts of data.

During the meta testing phase, test task T^{test} is extracted from the test task set $D^{\text{meta-test}}$. Similarly, the data in each test task T_i^{test} are partitioned into a query set T_{qi}^{test} and a support set T_{si}^{test}.

In this phase, the optimized parameters and model obtained in the meta training stage are finetuned through T_{si}^{test}. The parameters in the model are updated again through Equation (30) to obtain the final θ_i^*:

$$\theta_i^* = \theta - \gamma \nabla L_{T_{si}^{\text{test}}}(f_\theta) \tag{30}$$

where γ denotes the learning rate.

The loss function is as follows:

$$L(f_\theta) = -\frac{1}{N_s} \sum_{i=1}^{N_s} y_i \log f_\theta(x_i) \tag{31}$$

where x_i is the input feature of the model, y_i is the input label of the model, and N_s is sample size.

Finally, the model is validated by the data from T_{qi}^{test}.

Figure 2 shows the MAML network structure.

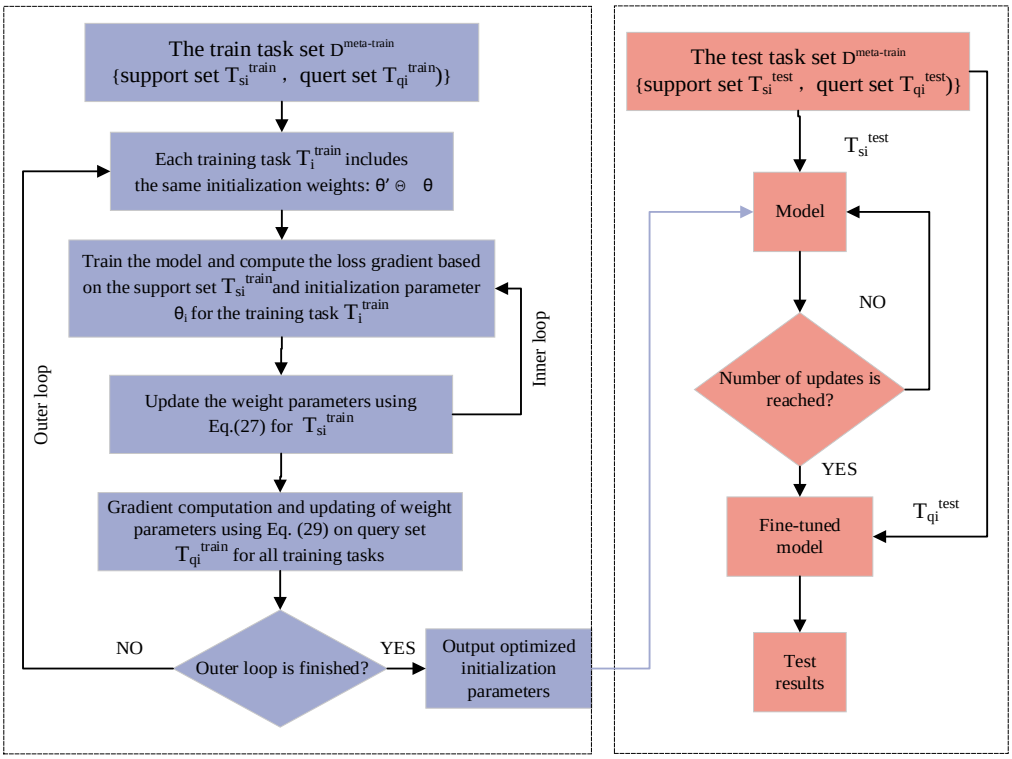


Figure 2. Network structure of MAML.

4.2.2. SAM

When processing sequence data, each element can be associated with other elements in the sequence, rather than just relying on the element itself. SAM can be used in deep learning to capture the interrelationships between elements in a sequence.

The structure of SAM is shown in Figure 3. It provides an efficient method for modeling and capturing information about the correlations between different tasks through the trio of the key, query, and value vector.

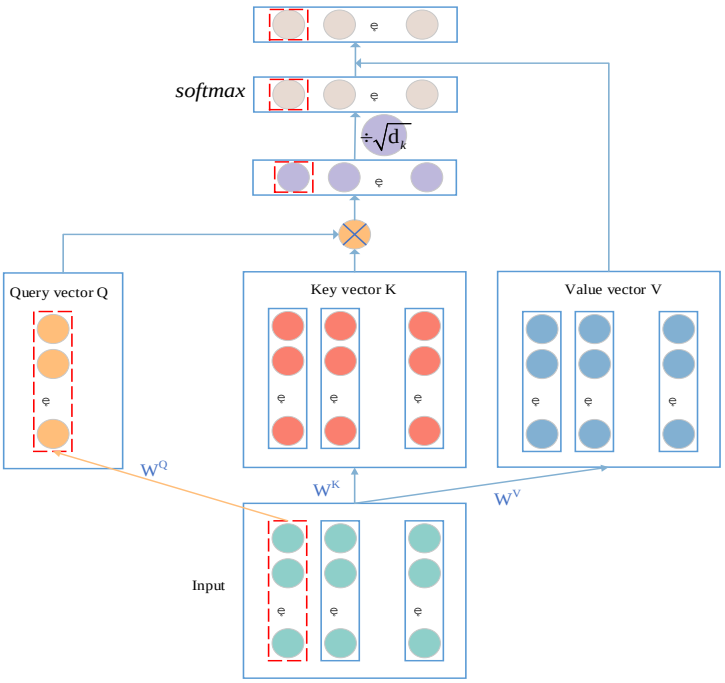


Figure 3. Structure diagram of SAM.

First, each input is linearly mapped to three different spaces. For the entire input sequence S, the query vector Q, key vector K, and value vector V are obtained through a linear mapping matrix [33]. The mapping process is illustrated below:

$$Q = S \cdot W^Q \tag{32}$$

$$K = S \cdot W^K \tag{33}$$

$$V = S \cdot W^V \tag{34}$$

where S represents the input vector. W^Q, W^K, and W^V represent the weight vectors.

Next, the dot product is applied to Q and K^T, where the dimensions of Q and K are the same. The results of the dot product undergo a scaling operation to yield similarity weight coefficients. These coefficients are then normalized using the softmax function.

Finally, the normalized similarity weight coefficient matrix is subjected to a dot product with vector V to obtain the attention score (AS).

$$AS = \text{softmax}(\frac{Q \cdot K^T}{\sqrt{d_k}}) \cdot V \tag{35}$$

where K^T is the transpose matrix of K, and $\sqrt{d_k}$ is the scaling factor.

The attention score allows us to quantify the degree of correlation between elements in a sequence.

Although MAML has shown its potential in deep learning, it has a core flaw: it cannot learn an initialization parameter that considers the correlation between tasks. This means that the initialization parameters of MAML may not always be optimal, especially when there is potential similarity between tasks. To overcome this problem, this article incorporates SAM into MAML. Compared with traditional MAML methods, it calculates the similarity between tasks based on the feature vectors output of each task in the network structure, thereby obtaining a more suitable initialization parameter that not only integrates information from the current task, but also incorporates information from other, similar tasks. In this way, an initialization parameter is generated which is more conducive to meta learning. This means that the designed network model is not only better able to learn individual tasks, but it also understands the interrelationships between tasks, thereby achieving a more efficient and accurate form of meta learning.

4.3. MAML-SAM-CNN-LSTM Network

This article adopts MAML-SAM as the meta learning framework. Under the guidance of MAML-SAM, considering the task's relevance, the optimal initialization parameters of the target network, CNN-LSTM, are found, and the interval solution of the weight coefficients is completed by MAML-SAM-CNN-LSTM. The network structure is shown in Figure 4.

Firstly, based on the different weight coefficients ω, their corresponding total cost, and the valley–peak coefficient (F, δ) are calculated by the wind–thermal–storage power system model. The data in the (F, δ) dataset are divided into intervals; then, a meta training set (including n training tasks) and a meta testing set are constructed.

During the meta-training phase, spatio-temporal features are extracted from each training task using CNN-LSTM. These feature vectors are input into the self-attention layer, and are weighted and rearranged for each task through a self-attention mechanism that excels at capturing the interrelationships between elements. This process optimizes the feature representations for each task, and the resulting optimized feature representations are utilized to update the model parameters in the subsequent two stages. In the first step, leveraging the support set data, the model parameters are adjusted at the individual task level according to Equation (27) for rapid adaptation to the new task. In the second step, using the query set data, the learning results from multiple tasks are aggregated to further optimize the initial model parameters through Equation (29). After two gradient updates,

MAML can learn the optimal initialization weights during the meta-training phase. This enables the model to achieve improved results not only on individual tasks but also across all tasks, facilitating enhanced generalization even in the face of unknown tasks.

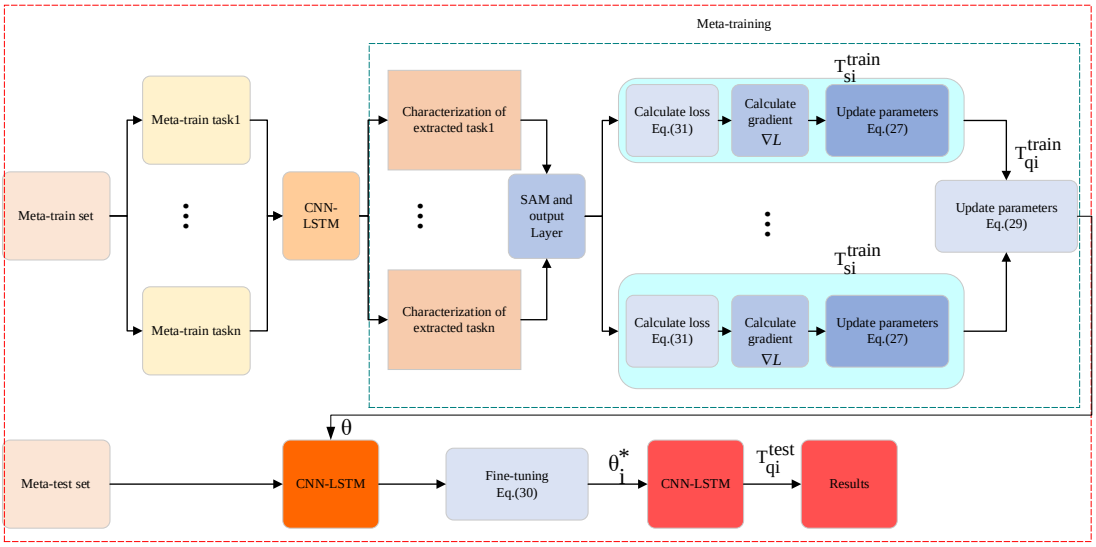


Figure 4. Network structure of MAML-SAM-CNN-LSTM.

During the meta-testing phase, the pre-optimized parameters are incorporated into the CNN-LSTM network. Subsequently, fine-tuning takes place using the support set Ttest si of the new task, enabling the model to better adapt to the characteristics of the specific task. After fine-tuning, validation is carried out using the query set Ttest qi of the new task to assess the generalization ability and performance of the model.

In this framework, the utilization of SAM facilitates the capture of intrinsic correlations and differences across tasks, thereby augmenting the model's feature extraction and learning capabilities. Within the scope of this paper, SAM is applied in the meta-training phase to enable the model to acquire the optimization parameters that are applicable to all tasks. However, in the meta-testing phase, the model requires only additional fine-tuning and validation on a specific task based on the optimization parameters, rendering the use of the self-attention mechanism unnecessary during this phase.

4.4. Algorithm Evaluation Indicators

This article uses accuracy (ACC), precision (PRE), recall (REC), and F1 score (F1) as the criteria to evaluate the performances of the MAML-SAM-CNN-LSTM network. The calculation methods for these evaluation indicators are thoroughly explained in Ref. [34].

5. Example Verification

This article employs a modified IEEE 30-node system for simulation analysis. The system includes six conventional, coal-fired thermal power generators, a wind farm located at node 8, a battery storage system, and multiple electric loads, as depicted in Figure 5 (Ⓦ represents the wind farm, ~ represents the thermal power unit, Ⓢ represents the battery storage system). The battery storage system is configured similarly to the largest energy storage project in China, featuring a capacity of 100 MW/400 MW·h. The parameters of thermal power units are taken from reference [35]. The 24 h load forecasting curve and wind power forecasting curve are shown in Figure 6. The time step is 1 h, during which power generation and load are considered constant.

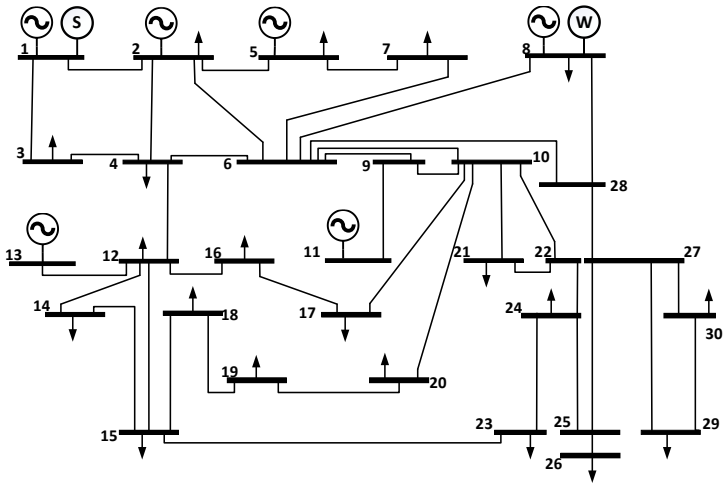


Figure 5. A modified IEEE 30-node system.

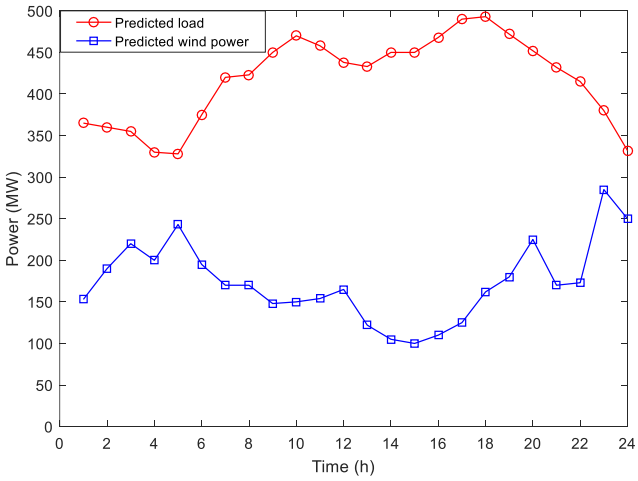


Figure 6. 24 h forecast curves of load and wind power.

5.1. Dynamic Adjustment of Weight Coefficients

To analyze the impacts of different attributes weights on each objective (system economy and peak load shifting in this paper) in the multi-objective optimization decision space, comparative analyses of the system operation results are conducted under different weight coefficients. The changes in the system's total costs and the net load valley–peak coefficients are shown in Figure 7, and some data are shown in Table 1.

Table 1. Total costs and net load valley–peak coefficients under various weight coefficients.

Weight Coefficient	System Total Cost (¥)	Net Load Valley–Peak Coefficient δ (%)
ω = 0	264,307.38	55.15
ω = 10	1,149,804.81	94.08
ω = 20	1,352,014.56	96.19

When the weight coefficient ω varies within the range of 0–20, both the total cost and the valley–peak coefficient of the net load rapidly increase as ω increases. When ω increases from 0 to 20, δ increases from 55.15% to 96.19%, and the valley–peak difference of the net load narrows. This indicates that the larger the weight coefficient, the more prominent the peak load shifting goals of the wind–thermal–storage hybrid system, and the better the improvement in the fluctuations in the net load curve. However, with ω increasing,

the total cost also shows an upward trend, indicating that good peak load shifting effects are directly proportional to the economic costs. When ω increases from 0 to 20, the total economic cost increases by more than five times, from 264,307.38 CNY to 1,352,014.56 CNY, which is mainly due to the gradual increase in system wind abandonment under the same storage capacity, in order to minimize the impact of the anti-peaking characteristics of the wind power and to obtain a smoother net load curve. When ω exceeds 20, δ levelled off, but the total cost still increases, so it is not discussed.

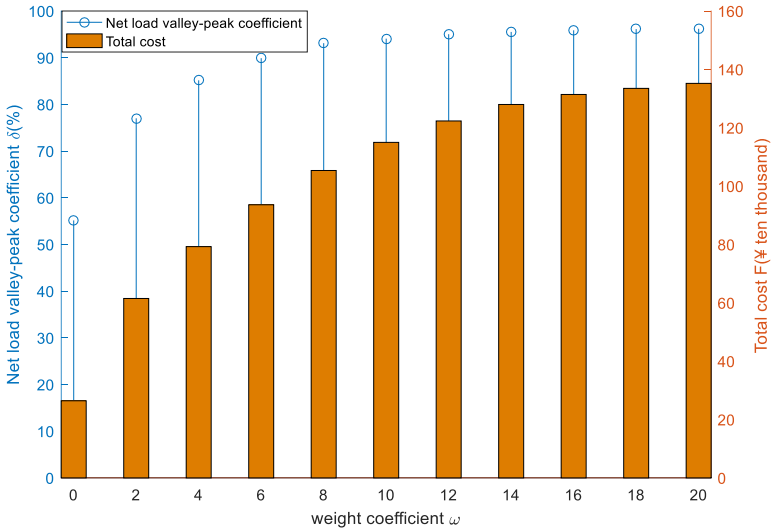


Figure 7. Total costs and net load valley–peak coefficients under various weight coefficients.

In summary, it can be seen that different system economy and peak load shifting effects can be obtained by changing the weight coefficient ω. Therefore, setting different weight coefficients based on operator preferences can allow for better control and management of the wind–thermal–storage system.

5.2. Solution Interval of Weight Coefficient

To address the interval range of the weight coefficient, we partition the sample dataset into ten tasks and one of them is randomly selected as the test task, while the remaining nine tasks serve as training tasks, to complete the training of the MAML-SAM-CNN-LSTM network.

Assume that the system operation indicators set by the operator are as follows: the net load valley–peak coefficient is above 80%, and the total daily operating cost is below 800,000 CNY, i.e., (F, δ) = (800,000, 80%). Inputting this into the trained MAML-SAM-CNN-LSTM network, the weight coefficients that meet the requirements can be directly obtained, which is a range described in [2.74, 4.09]. The changes in the system net load, actual output of the wind farm, and the energy storage power when the weight coefficients are taken from both ends are shown in Figure 8.

When ω = 2.74, the peak–valley difference in the net load is 63.2 KW, and the valley–peak coefficient of the net load is 80.06%. When ω increases to 4.09, the peak–valley difference decreases to 45.4 KW, and the valley–peak coefficient increases to 85.37%. The net load curve of the system becomes smoother, indicating that the value of ω affects the fluctuation level of the system's net load. The larger the value of ω, the more stable the net load curve. However, at the same time, better peak load shifting effects will lead to an increase in wind abandonment, resulting in a higher total cost. On the contrary, the smaller the value of ω, the lower the economic cost of the system.

To further verify the accuracy of the weight coefficient range provided by the MAML-SAM-CNN-LSTM network, extreme and intermediate values are taken and substituted into the wind–thermal–storage system model for verification. The total system costs and net load valley–peak coefficients are shown in Table 2.

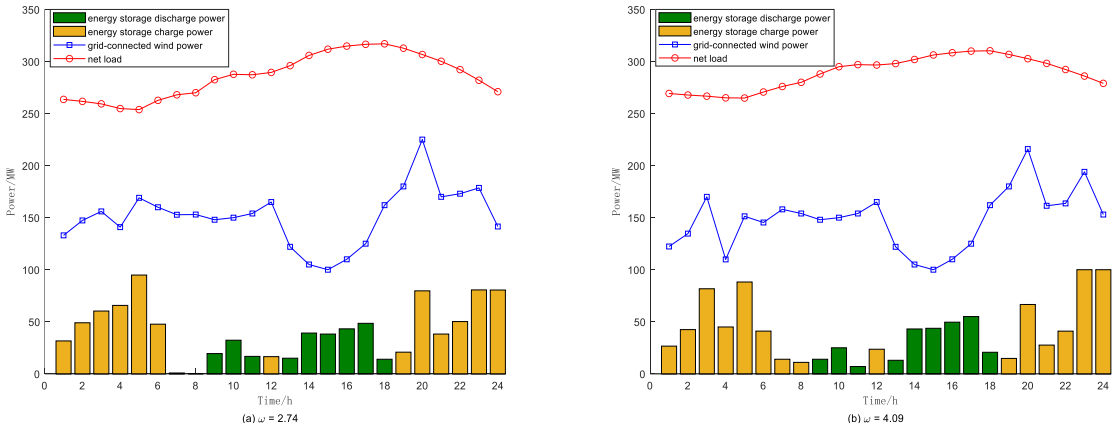


Figure 8. Power curves when weight coefficient takes the values at its interval endpoints.

Table 2. Optimization results of the wind–thermal–storage system under different weights.

Weight Coefficient	System Total Cost (CNY)	Net Load Valley-Peak Coefficient δ (%)
ω = 2.73	679,321.10	79.97
ω = 2.74	681,273.51	80.06
ω = 3.42	741,798.09	82.83
ω = 4.09	798,866.43	85.37
ω = 4.10	800,442.88	85.42

When the weight coefficient is less than the lower limit of the solution range, it may be appropriate to assume ω = 2.73. Although the total system cost is below 800,000 CNY, the net load valley–peak coefficient is 79.97%, and does not meet the requirements of the peak load shifting indicators. As the larger the value of ω, the better the peak load shifting effects, when ω is less than 2.73, the net load valley–peak coefficient will not meet the indicator requirements set by the operator.

When the weight coefficient value exceeds the upper limit of the solution range, it may be appropriate to take ω = 4.10. At this point, the net load valley–peak coefficient is 85.42%, which meets the requirements, but the total system cost has exceeded 800,000 CNY. Because total cost increases with the increase in ω, when ω is greater than 4.10, the system cannot meet the economic indicators.

When the value of ω falls within the range of 2.74–4.09, both the peak load shifting effect indicator and the economic indicator are within the range required by the operator. The findings illustrate the accuracy and feasibility of the proposed MAML-SAM-CNN-LSTM network model in solving the weight coefficient interval, which can adjust the weight coefficients according to the operator's preferences, coordinate the system's peak load shifting effects and economy as needed, and assist in scheduling to achieve optimal decision-making.

5.3. Comparison of Different Network Models

5.3.1. Experimental Data Design

Due to the different dimensions of total cost and the valley–peak coefficient, normalization is required, as follows:

$$x_{norm} = \frac{x_i - x_{min}}{x_{max} - x_{min}} \quad (36)$$

where x_i is a data point in the original dataset. x_{max} and x_{min} are the maximum and minimum values of the original dataset, respectively. x_{norm} is the normalized value of x_i, with a range of [0, 1].

For the meta learning model, dataset partitioning is required. The value range of the weight coefficients [0, 20] is divided into 10 equal parts, forming a pattern of [0, 2], (2, 4], . . ., (18, 20]. The data in the database corresponding to each equal part are divided into 1 task, totaling 10 tasks. To verify the classification performances of several network models regarding extreme values, three different training and testing tasks are established, as shown in Table 3. The first method is to use T_1 as the testing task and other data as the training task; The second type uses T_{10} as the testing task and other data as the training task. The third type uses T_5 as the testing task and other data as the training task. The data in each task are further partitioned, forming support and query sets.

Table 3. Data partitioning.

Training Task Sets	Testing Task Sets
T_2, T_3,. . .,T_{10}	T_1
T_1, T_2,. . ., T_9	T_{10}
T_1,. . ., T_4, T_6,. . ., T_{10}	T_5

5.3.2. Comparison of Performances

Four models, LSTM, CNN-LSTM, MAML-CNN-LSTM, and MAML-SAM-CNN -LSTM, are used to solve the weight coefficients, and their performance evaluations are presented. Tables 4–6 show the evaluation results.

Table 4. Performance evaluation results of LSTM and CNN-LSTM.

Tested Model	ACC	PRE	REC	F1
LSTM	88.07%	87.02%	86.96%	86.99%
CNN-LSTM	90.86%	90.60%	89.13%	89.86%

Table 5. Performance evaluation results of MAML-CNN-LSTM.

Testing Task	ACC	PRE	REC	F1
T_1	95.24%	95.59%	94.12%	94.85%
T_{10}	95.45%	94.74%	92.11%	93.41%
T_5	95.24%	94.12%	91.18%	92.63%

Table 6. Performance evaluation results of MAML-SAM-CNN-LSTM.

Testing Task	ACC	PRE	REC	F1
T_1	98.73%	98.61%	99.07%	98.84%
T_{10}	98.73%	98.95%	98.30%	98.62%
T_5	98.72%	98.57%	98.57%	98.57%

By comparison, it can be found that the LSTM model has the lowest scores for four indicators (accuracy, precision, recall rate, and F1 score) indicating that a single deep learning algorithm has an average performance in handling complex tasks. The performance of the CNN-LSTM model is slightly better than that of the LSTM model, but there is no significant difference. The MAML-CNN-LSTM model, due to its use of meta learning algorithms that have the advantage of processing small sample data, significantly improves prediction accuracy, but still performs slightly worse than the MAML-SAM-CNN-LSTM model.

The MAML-SAM-CNN-LSTM model achieves an excellent performance in all four indicators and is not affected by different training and testing tasks. Compared to the LSTM model, the accuracy improved by 12.10%, and the average F1 score increased by 13.44%.

Compared to the MAML-CNN-LSTM model, the average accuracy also increased by 3.59%, and the average F1 score increased by 5.39%. These data further verify the superiority of the model proposed in this paper. Due to the use of MAML as the training framework, this model is good at handling small sample problems, and SAM is used to fully explore the relevant features of various tasks, causing this model to have an efficient learning speed and a good generalization ability, which is conducive to achieving a more accurate solution of weight coefficients.

6. Conclusions

This article proposes a method for solving the weight coefficient interval in multi-objective optimization problems. Taking the operation optimization of the hybrid power system as an example, the goal is set to minimize the total cost, and the peak load shifting goal is converted into the economic cost of load-balancing and added to the total cost. A wind–thermal–storage system optimization model is established, and then a deep learning network is designed to solve the feasible weight coefficient range, achieving the goal of the multi-objective optimization of the system. For small sample datasets, SAM is integrated into MAML to guide the target network, CNN-LSTM, to find initial optimization parameters that consider the task's relevance, thereby accurately achieving an interval solution of weight coefficients. Through numerical simulation, the results show the following:

(1) Given the threshold of operating indicators for the wind–thermal–storage system, the MAML-SAM-CNN-LSTM network model can correctly solve the weight coefficient interval so that it meets the operation requirements and preferences for the multi-objective optimization model, indicating that the proposed network model is feasible and accurate.
(2) In different training and testing tasks, the MAML-SAM-CNN-LSTM model has achieved an excellent performance, and the mean values of evaluation indicators, such as accuracy, precision, recall rate, and F1 score, reach 98.73%, 98.71%, 98.65%, and 98.68%, respectively, demonstrating its good adaptability.
(3) The accuracy of the MAML-SAM-CNN-LSTM network is improved by about 12.10% compared to a single LSTM model. Compared to the MAML-CNN-LSTM model, it also improves by about 3.59%, indicating that the proposed network model is superior and can more accurately optimize the weight coefficient interval, thereby assisting scheduling in achieving optimal decision-making.

Author Contributions: Y.L.: conceptualization, methodology, software, data curation, visualization, investigation, writing—original draft preparation, reviewing and editing. M.P.: conceptualization, methodology, supervision, and writing—reviewing. All authors have read and agreed to the published version of the manuscript.

Funding: This research was supported in part by the National Natural Science Foundation of China under Grant 61973107 and Grant 61472128.

Data Availability Statement: The datasets and materials used in this study are available upon request. Interested researchers can contact Yanchen Liu at liuyanchen@hnu.edu.cn to request access to the data and materials used in this study.

Acknowledgments: The authors extend their heartfelt appreciation to the reviewers and editors for their invaluable comments and constructive suggestions.

Conflicts of Interest: The authors declare that they have no known competing financial interests or personal relationships that could have appeared to influence the work reported in this paper.

References

1. Akram, U.; Khalid, M.; Shafiq, S. Optimal Sizing of a Wind/Solar/Battery Hybrid Grid-connected Microgrid System. *Iet. Renew. Power Gener.* **2017**, *12*, 72–80. [CrossRef]
2. Yu, X.B.; Duan, Y.C.; Luo, W.G. A knee-guided algorithm to solve multi-objective economic emission dispatch problem. *Energy* **2022**, *259*, 124876. [CrossRef]
3. Wang, B.; Zhou, M.; Xin, B.; Zhao, X.; Watada, J. Analysis of operation cost and wind curtailment using multi-objective unit commitment with battery energy storage. *Energy* **2019**, *178*, 101–114. [CrossRef]
4. Patwal, R.S.; Narang, N. Multi-objective generation scheduling of integrated energy system using fuzzy based surrogate worth trade-off approach. *Renew. Energy* **2020**, *156*, 864–882. [CrossRef]
5. He, Y.; Guo, S.; Zhou, J.X.; Ye, J.L.; Huang, J.; Zheng, K.; Du, X.R. Multi-objective planning-operation co-optimization of renewable energy system with hybrid energy storages. *Renew. Energy* **2022**, *184*, 776–790. [CrossRef]
6. Baghaee, H.R.; Mirsalim, M.; Gharehpetian, G.B.; Talebi, H.A. Reliability/cost-based multi-objective Pareto optimal design of stand-alone wind/PV/FC generation microgrid system. *Energy* **2016**, *115*, 1022–1041. [CrossRef]
7. Xiao, H.Q.; He, H.L.; Zhang, L.D.; Liu, T. Adaptive Grid-Synchronization Based Grid-Forming Control for Voltage Source Converters. *IEEE Trans. Power Syst.* **2023**, 1–4. [CrossRef]
8. Guo, Z.H.; Zhang, R.; Wang, L.; Zeng, S.Q.; Li, Y.J. Optimal operation of regional integrated energy system considering demand response. *Appl. Therm. Eng.* **2021**, *191*, 116860. [CrossRef]
9. Mohamed, F.A.; Koivo, H.N. Multiobjective optimization using modified game theory for online management of microgrid. *Eur. Trans. Electr. Power* **2011**, *21*, 839–854. [CrossRef]
10. Han, X.J.; Wang, F.; Tian, C.G.; Xue, K.; Zhang, J.F. Economic Evaluation of Actively Consuming Wind Power for an Integrated Energy System Based on Game Theory. *Energies* **2018**, *11*, 1476. [CrossRef]
11. Li, X.Z.; Wang, W.Q. Dynamic Environmental Economic Dispatch of Wind Farm Based on Multi-objective Moth-flame Optimization. *J. Electr. Eng.* **2020**, *15*, 1–12. [CrossRef]
12. Mayer, M.J.; Szilagyi, A.; Grof, G. Environmental and economic multi-objective optimization of a household level hybrid renewable energy system by genetic algorithm. *Appl. Energy* **2020**, *269*, 115058. [CrossRef]
13. Hosseinnia, H.; Modarresi, J.; Nazarpour, D. Optimal eco-emission scheduling of distribution network operator and distributed generator owner under employing demand response program. *Energy* **2020**, *191*, 116553. [CrossRef]
14. Dorotić, H.; Pukšec, T.; Duić, N. Economical, environmental and exergetic multi-objective optimization of district heating systems on hourly level for a whole year. *Appl. Energy* **2019**, *251*, 113394. [CrossRef]
15. Lu, J.X.; Wang, W.J.; Zhang, Y.C.; Cheng, S. Multi-objective optimal design of stand-alone hybrid energy system using entropy weight method based on HOMER. *Energies* **2017**, *10*, 1664. [CrossRef]
16. Zhang, X.C.; Zhu, J.D.; Yang, D.M.; Chen, Y.H.; Du, W. Research on Operational Optimization Technology of Regional Integrated Energy System Considering Operating Cost and Reliability. In Proceedings of the 4th International Forum on Smart Grid Protection and Control, Nanjing, China, 17–18 August 2019. [CrossRef]
17. Li, P.; Ma, J.; Zhao, B. Game theory method for multi-objective optimal Operation of Microgrid. In Proceedings of the General Meeting of the IEEE-Power-and-Energy-Society, Denver, CO, USA, 26–30 July 2015. [CrossRef]
18. Wang, Q.Q.; Zeng, J.; Liu, J.F.; Chen, J.L.; Wang, Z.G. A Distributed Multi-objective Optimization Algorithm for Resource-storage-load Interaction of Microgrid. *Proc. CSEE* **2020**, *40*, 1421–1432. [CrossRef]
19. Liu, R.H.; Yang, T.; Sun, G.P.; Lin, S.F.; Li, F.; Wang, X. Multi-Objective Optimal Scheduling of Community Integrated Energy System Considering Comprehensive Customer Dissatisfaction Model. *IEEE Trans. Power Syst.* **2023**, *38*, 4328–4340. [CrossRef]
20. Ren, X.Y.; Bu, X.H.; Yin, Y.L.; Liu, J.H. Coordinated and Optimal Dispatching for Wind-Photovoltaic-Storage Systems Based on Multi-Strategy Multi-Objective Differential Evolution Algorithm. *J. Syst. Simul.* 2023, *online publishing*. [CrossRef]
21. Luo, Y.; Zhang, Y. Day-ahead scheduling of wind-solar-pumped storage system based on predictive variation multi-objective particle swarm optimization. *Renew. Energy Resour.* **2023**, *41*, 1484–1490. [CrossRef]
22. Xiao, H.Q.; Gan, H.C.; Yang, P.; Li, L.F.; Li, D.; Hao, Q.R.; Huang, Y.; Dai, L.S.; Liu, Y.L. Robust submodule fault management in modular multilevel converters with nearest level modulation for uninterrupted power transmission. *IEEE Trans. Power Deliv.* **2023**, 1–16. [CrossRef]
23. Dhiman, G.; Singh, K.K.; Soni, M.; Nagar, A.; Dehghani, M.; Slowik, A.; Kaur, A.; Sharma, A.; Houssein, E.H.; Cengiz, K. MOSOA: A New Multi-objective Seagull Optimization Algorithm. *Expert Syst. Appl.* **2021**, *167*, 114150. [CrossRef]
24. Lian, J.J.; Zhang, Y.S.; Ma, C.; Yang, Y.; Chaima, E. A review on recent sizing methodologies of hybrid renewable energy systems. *Energy Convers. Manag.* **2019**, *199*, 112027. [CrossRef]
25. Gan, L.W.; Topcu, U.; Low, S.H. Optimal decentralized protocol for electric vehicle charging. *IEEE Trans. Power Syst.* **2013**, *28*, 940–951. [CrossRef]
26. LeCun, Y.; Bottou, L.; Bengio, Y.; Haffner, P. Gradient-based learning applied to document recognition. *Proc. IEEE* **1998**, *86*, 2278–2324. [CrossRef]
27. Bengio, Y.; Simard, P.; Frasconi, P. Learning long-term dependencies with gradient descent is difficult. *IEEE Trans. Neural. Netw.* **1994**, *5*, 157–166. [CrossRef]
28. Zhou, C.J.; Wang, Y.J.; Li, K.Q.; Chen, Z.H. State of Health Estimation for Lithium-Ion Battery Based on Gray Correlation Analysis and Long Short-Term Memory Neural Network. *Trans. China Electrotech. Soc.* **2022**, *37*, 6065–6073. [CrossRef]

29. Wang, Y.X.; Yan, J.; Wang, J.H.; Geng, Y.S. Few-Shot Partial Discharge Diagnosis for Gas-Insulated Switchgear Using a Novel Multi-Level Second-Order Attention Siamese Network. *Trans. China Electrotech. Soc.* **2023**, *38*, 2255–2264. [CrossRef]
30. Finn, C.; Abbeel, P.; Levine, S. Model-agnostic meta-learning for fast adaptation of deep networks. In Proceedings of the 34th International Conference on Machine Learning, Sydney, Australia, 6–11 August 2017. [CrossRef]
31. Raghu, A.; Raghu, M.; Bengio, S.; Vinyals, O. Rapid learning or feature reuse? Towards Understanding the Effectiveness of MAML. In Proceedings of the International Conference on Learning Representations, Addis Ababa, Ethiopia, 26–30 April 2020. [CrossRef]
32. Zhong, L.L.; Wu, B.Y.; Wu, Q. Numerical Solution of Electron Boltzmann Equation in Gas Discharge Plasmas Based on Meta Learning. *Trans. China Electrotech. Soc.* **2023**, 239621. [CrossRef]
33. Ju, Y.; LI, J.; Sun, G.Y. Ultra-Short-Term Photovoltaic Power Prediction Based on Self-Attention Mechanism and Multi-Task Learning. *IEEE Access* **2020**, *8*, 44821–44829. [CrossRef]
34. Yildirim, O.; Baloglu, U.B.; Tan, R.S.; Ciaccio, E.J.; Acharya, U.R. A new approach for arrhythmia classification using deep coded features and LSTM networks. *Comput. Methods Programs Biomed.* **2019**, *176*, 121–133. [CrossRef]
35. Huang, Y.; Hu, W.; Min, Y.; Luo, W.H.; Wang, Z.M.; Ge, W.C. Multi-objective coordinative dispatch for wind-storage combined systems considering day-ahead generation schedules. *Proc. CSEE* **2014**, *34*, 4743–4751. [CrossRef]

Disclaimer/Publisher's Note: The statements, opinions and data contained in all publications are solely those of the individual author(s) and contributor(s) and not of MDPI and/or the editor(s). MDPI and/or the editor(s) disclaim responsibility for any injury to people or property resulting from any ideas, methods, instructions or products referred to in the content.